ORIGINAL PAPER

Mechanical Properties and Failure Behavior of Dry and Water-Saturated Anisotropic Coal Under True-Triaxial Loading Conditions

Yubing Liu[1,2,3] · Guangzhi Yin[1,2] · Minghui Li[1,2,4] · Dongming Zhang[1,2] · Gun Huang[1,2] · Peng Liu[1,2] · Chao Liu[1,2] · Honggang Zhao[1,2] · Beichen Yu[1,2]

Abstract

In underground coal mining, coal failure generally occurs due to the relatively weak strength of the coal and the high applied mining-induced stresses. The outer complex geological conditions (i.e., tectonic structure and water intrusion) and internal structural anisotropy of the coal introduce uncertainty in predicting its mechanical properties and failure behavior. In this study, laboratory investigations of the mechanical properties and failure behavior of dry and water-saturated anisotropic coal samples subjected to different true-triaxial loading stresses were conducted. The effects of water weakening, intermediate stress, and structural anisotropy on the mechanical properties and failure behavior of the coal were systematically studied. The results indicate that the presence of water significantly reduced the strength, elastic modulus, and strength anisotropy of the coal. The maximum stress at failure first increased and then decreased with increasing intermediate stress. The residual strength-to-peak strength ratios and failure plane angles of the coal showed a linear increase with increasing intermediate stress. When the coal samples were loaded in the bedding plane direction, the brittleness of the coal was higher than when they were loaded in the other two cleat plane directions. In addition, when the coal samples were loaded in the butt cleat plane direction, the brittleness of the coal decreased with increasing intermediate stress. Two typical failure modes of the dry and water-saturated coal samples were observed: shear and mixed splitting and shear failures. The dominant failure mode of the coal also varied with the loading direction relative to the weakness planes, which could be well recognized and predicted by the acoustic emission (AE) characteristic curves. To further reveal the fracture mechanism, the microcrack patterns of the coal were further identified based on the AE parameters.

Keywords Mechanical properties · Failure modes · Water weakening · True-triaxial stress · Anisotropic coal

✉ Yubing Liu
  liuyb@cqu.edu.cn

✉ Minghui Li
  mhli@cqu.edu.cn

1 State Key Laboratory of Coal Mine Disaster Dynamics and Control, Chongqing University, Chongqing 400030, China

2 School of Resources and Safety Engineering, Chongqing University, Chongqing 400030, China

3 Department of Exploration Geophysics, Curtin University, 26 Dick Perry Avenue, Kensington 6151, Australia

4 Guangdong Provincial Key Laboratory of Deep Earth Sciences and Geothermal Energy Exploitation and Utilization, Institute of Deep Earth Sciences and Green Energy, College of Civil and Transportation Engineering, Shenzhen University, Shenzhen 518060, China

List of Symbols

σ_1	The maximum stress
σ_2	The intermediate stress
σ_3	The minimum stress
E	Elastic modulus
M	Postpeak modulus
v	Poisson's ratio
x	The distance into the coal pillar
h	The coal pillar height
B_1, B_2	The brittleness index
W_r	The postpeak rupture energy
W_e	The elastic energy
W_a	The released energy

1 Introduction

Coal, as a heterogeneous fractured rock, has relatively low strength. When subjected to high stress, coal can undergo progressive failure (Wang et al. 2013). The failure behavior of coal depends on mechanical properties (e.g., the strength, anisotropy, and brittleness) and can also be reflected by acoustic emissions (AEs) (Li et al. 2019; Kong et al. 2016; Liu et al. 2019c, d; Duan et al. 2019). In underground coal mining, mining-induced stress concentration can easily lead to failure of the coal. With the increasing depth of mining operations, more complex support methods are needed, and the associated mining hazards are also more pronounced (Mark and Gauna 2016; Zhao et al. 2018). Knowledge of the mechanical properties and failure behavior of coal during the evolution from deformation to failure is of vital importance to coal support design and coal burst control.

Laboratory experimental tests can provide links to field observations and theoretical predictions. However, how to better replicate in situ conditions in the laboratory is still challenging. With regard to stress replication, extensive uniaxial and conventional stress tests have been performed on the mechanical properties and failure behavior of coal and rock (Prikryl et al. 2003; Liu et al. 2018a, b, 2019c, d; Yang et al. 2012; Xu et al. 2018; Yin et al. 2015; Zhang et al. 2018a, b). Various in situ stress measurements indicate that the uniaxial and conventional stress conditions are rarely found, while true-triaxial stress conditions ($\sigma_1 > \sigma_2 > \sigma_3$) are more general in the crust (Zoback 1992; Kang et al. 2010; Paul and Chatterjee 2011). Limited true-triaxial stress tests on the mechanical properties and failure behavior of specific sedimentary rock are found in the literature (Ma and Haimson 2016; Browning et al. 2017; Kong et al. 2018; Lu et al. 2018; Li et al. 2018). However, to the best of our knowledge, no such true-triaxial stress experimental tests have been performed on coal.

In comparison with other rocks, natural discontinuity is more complex in coal with numerous cleats and bedding planes. Geometrically, the cleats and bedding planes are mutually perpendicular (Laubach et al. 1998). The cleats and bedding planes have a great influence on the mechanical properties and failure behavior of coal (Ranjith and Perera 2012; Li et al. 2016; Zhang et al. 2018a, b; Scholtès et al. 2011). Experimental deviation could be significant when considering coal as an isotropic medium. In addition, coal seams are generally saturated with water, especially for the area treated by hydraulic stimulation. Experimental efforts have been devoted to investigating the influence of water on the mechanical properties and failure behavior of rock. The majority of these studies focused on the effect of water on the uniaxial and triaxial compressive strength (Wong et al. 2015; Li et al. 2012; Vásárhelyi and Van 2006) and the deformational and fracturing behavior (Minaeian et al. 2017; Kwasniewski and Rodríguez-Oitaben 2009; Wasantha and Ranjith 2014). In contrast to the numerous studies on rocks, only a few studies have explored the effect of water on the mechanical properties and failure behavior of coal (Zhao et al. 2016; Poulsen et al. 2014; Yao et al. 2016; Perera et al. 2011). However, the influence of anisotropy and the presence of water under true-triaxial compression, which represent a more realistic site environment, have not been taken into account.

In this paper, laboratory investigations of the mechanical properties and failure behavior of anisotropic coal using a newly developed true-triaxial apparatus were executed under both dry and water-saturated conditions. The effects of water weakening, intermediate stress, and anisotropy on the mechanical properties and failure behavior were systematically examined. The AE energy evolution of coal during progressive failure progress was discussed. The relationship between the failure mode of coal and AE characteristic curves was further analyzed. Microcrack patterns of coal were then classified based on the AE parameters. Finally, the potential field applications of the experimental results were discussed.

2 Experimental Methodology

2.1 Sample Description and Preparation

The coal samples used in this study were collected from working face 2461 of coal seam C1 of the Baijiao coal mine in Sichuan Province, China. The buried depth of the sampling location was approximately 580 m. The coal samples were obtained from the same coal block to maintain good consistency in physical and mechanical properties. The coal samples were processed as cubes with side lengths of 100 mm (± 0.02 mm) and with the surfaces ground flat and parallel to within ± 0.02 mm. To select intact samples, the prepared coal samples were scanned by X-ray computed tomography (CT) to remove the samples with macrofractures induced by sample preparation. The coal samples were identified by ASTM D388 as high-rank anthracites with a vitrinite reflectance of 2.85%. The ash and volatile matter contents measured on the crushed coal were 23.93% and 15.05%, respectively (Liu et al. 2019a, b). The bulk densities of the dry and water-saturated coal were 1.55 g/cm^3 and 1.58 g/cm^3, respectively. The basic mechanical parameters and mineral components of the coal samples are listed in Tables 1 and 2, respectively. Coal is a highly anisotropic porous medium induced by preexisting cleats and bedding planes; these microstructures are easily distinguished in

Table 1 Basic mechanical parameters of the anthracite coal samples (Liu et al. 2018a, b)

Orientation	UCS (MPa)	E (GPa)	v	Tensile strength (MPa)
Parallel to bedding	20.03	3.42	0.14	2.75
Perpendicular to bedding	25.28	2.95	0.22	1.95

UCS unconfined compressive strength, *E* elastic modulus, *v* Poisson's ratio

Table 2 Mineral components of the anthracite coal samples (Zhang et al. 2016)

	Kaolinite	Quartz	Calcite	Others
Mineral content (%)	5.58	11.74	5.04	77.64

Fig. 1. A total of 54 cubic coal samples were finally prepared. Half of the cubic coal samples were placed in a 105 °C drying oven for 24 h, and the rest were immersed in a water bath for 7 days. Both the dry and water-saturated cubic coal samples were separated into three groups based on the different true-triaxial stress conditions. To avoid the dispersion of test results by the heterogeneity of the coal samples, three tests were repeated for each true-triaxial stress condition.

2.2 Test Apparatus and Procedure

The true-triaxial test in this study was performed using a newly developed multifunctional true-triaxial geophysical (TTG) apparatus at Chongqing University in China. The apparatus can apply 3D stress levels of up to 600 MPa in two directions and 400 MPa in another direction. The deformation of the coal samples is measured by six linear variable differential transformers (LVDTs). Detailed descriptions of the TTG apparatus can be found in Li et al. (2016) and

Jiang et al. (2019). The lubricant made of petroleum jelly and stearic acid was applied to the surface of six loading plates to reduce the end friction effect between the loading plates and the cubic samples.

The 16-channel PCI-2 AE monitoring system from Physical Acoustic Corporation (PAC) was used to record the acoustic output during the experimental test. The AE sensors were embedded on the loading plate through the preopened installing holes and lead grooves, and the AE signal lines were drawn out from the sides of the loading plates, as shown in Fig. 2a. A total of eight AE sensors were mounted on the top and bottom faces of the specimen, as shown in Fig. 2b. Each AE sensor had a diameter of 5 mm and a monitoring frequency range of 100–900 kHz. The amplitude threshold of the AE sensors was set to 45 dB, and the preamplifier gain was selected to be 40 dB. The time parameters for AE waveforms such as peak definition time (PDT), hit definition time (HDT), and hit locking time (HLT) were set to 50, 100, and 100 μs, respectively.

All the tests followed the same designed stress path, as shown in Fig. 3a, which is also suggested by the International Society for Rock Mechanics (ISRM) (Feng et al. 2019). First, the coal sample was loaded hydrostatically (where $\sigma_1 = \sigma_2 = \sigma_3$) to the desired σ_3 at a rate of 0.5 MPa/s. Next, σ_3 was kept constant while increasing σ_1 and σ_2 simultaneously to the preset σ_2 at the rate of 0.5 MPa/s. Finally, σ_2 and σ_3 were maintained, while σ_1 was increased at the displacement rate of 0.002 mm/s until coal sample failure, which was characterized by a sudden drop in σ_1 followed by residual strength. The applied stress level of σ_3 was maintained at 10 MPa, while for each constant σ_3, the stress levels of σ_2 were 15, 20, and 30 MPa. The designed stress level could cover the stress conditions encountered in the studied area, since the measured in situ horizontal stresses were 17.25 and 28.70 MPa, respectively (Jia et al. 2006). Three loading directions were also designed in terms of mutually perpendicular preexisting microstructures (bedding plane, face cleat, and butt cleat) in coal, as schematically shown

Fig. 1 Prepared cubic coal sample
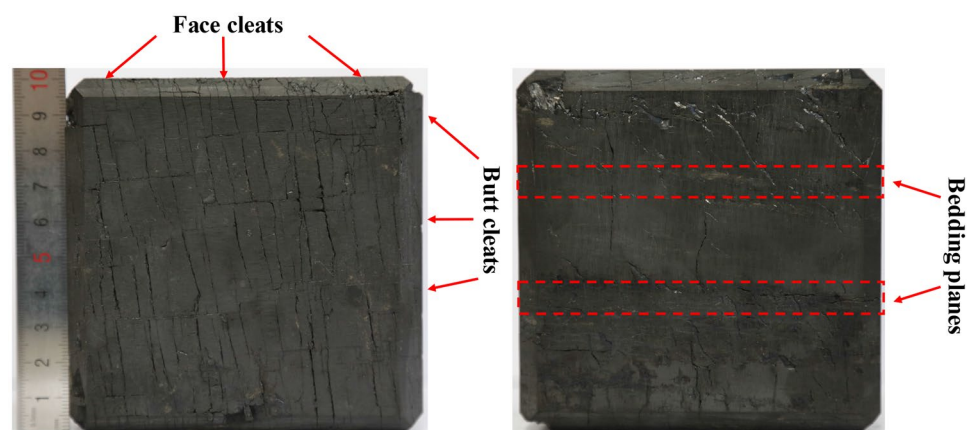
Fig. 2 Loading plate with mounted AE sensors and the location of AE sensors. **a** Loading plate and **b** location of AE sensors

AE sensors

AE signal lines

(a)

80 mm

AE sensor

80 mm

100 mm

Specimen

(b)
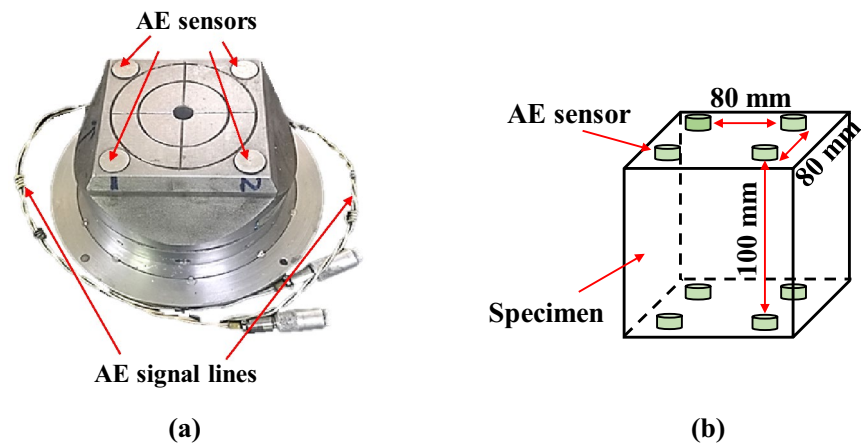
Fig. 3 Stress loading path and loading direction variations in the true-triaxial tests. **a** Stress loading path and **b** stress loading direction variations

(a)

Loading Direction 1

Loading Direction 2

Loading Direction 3

(b)
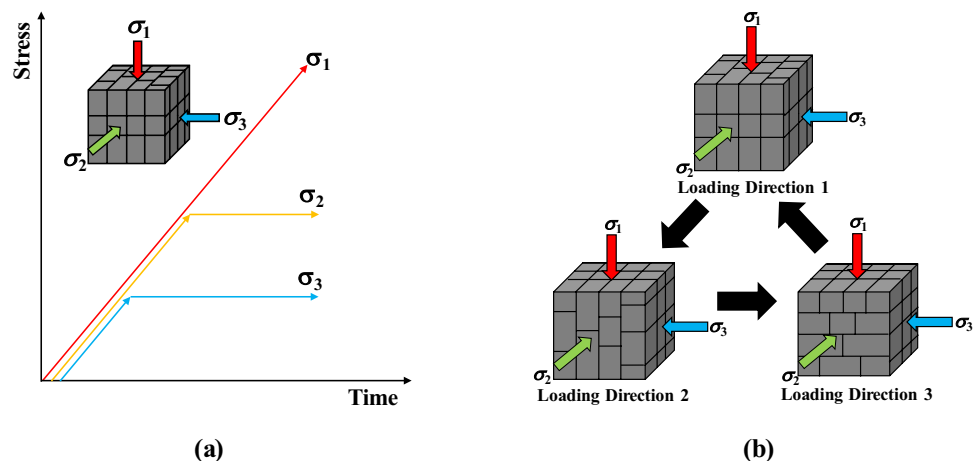
in Fig. 3b. In the loading direction 1, σ_1 is perpendicular to the bedding plane in the coal, while σ_1 is parallel to the face cleat and butt cleat planes in loading directions 2 and 3, respectively. After true-triaxial compression tests, all the cubic coal samples were scanned by X-ray CT to identify the fracture morphology and finial failure modes.

3 Results and Analysis

3.1 Differential Stress–Strain Curves of Dry and Water-Saturated Anisotropic Coal Samples

Figures 4 and 5 show plots of the axial strain against the maximum differential stress $(\sigma_1 - \sigma_3)$ for a fixed σ_3 value of 10 MPa, with variable σ_2 of the dry and water-saturated anisotropic coal samples. For all the tested coal samples, a noticeable stress drop followed by the strain-softening stage was observed, indicating that the coal samples present brittle failure modes under the true-triaxial stress loading range. Figures 4 and 5 show that the peak strength and initial slope of the stress–strain curve decreased significantly

after absorption of water for different true-triaxial loading conditions and directions. In terms of the effect of the intermediate principal stress, the peak strength increased first and then decreased with the increase in the difference between σ_2 and σ_3. According to the test data and the differential stress–strain curves of the coal samples, the peak and residual strength, the axial strain at failure point, and the elastic and postpeak modulus were obtained and are summarized in Table 3. The elastic modulus was determined as the slope of the differential stress–strain curve at half of the peak strength, while the postpeak modulus was calculated from the slope of the straight line that connects the points of the peak and residual strength.

3.2 Failure Modes of Dry and Water-Saturated Anisotropic Coal Samples

Figures 6 and 7 show the cross-sectional and 3D reconstruction images of failure modes of the dry and water-saturated anisotropic coal samples under different true-triaxial loading conditions. In the 3D reconstruction images, the fracture regions are white, and the remaining regions are
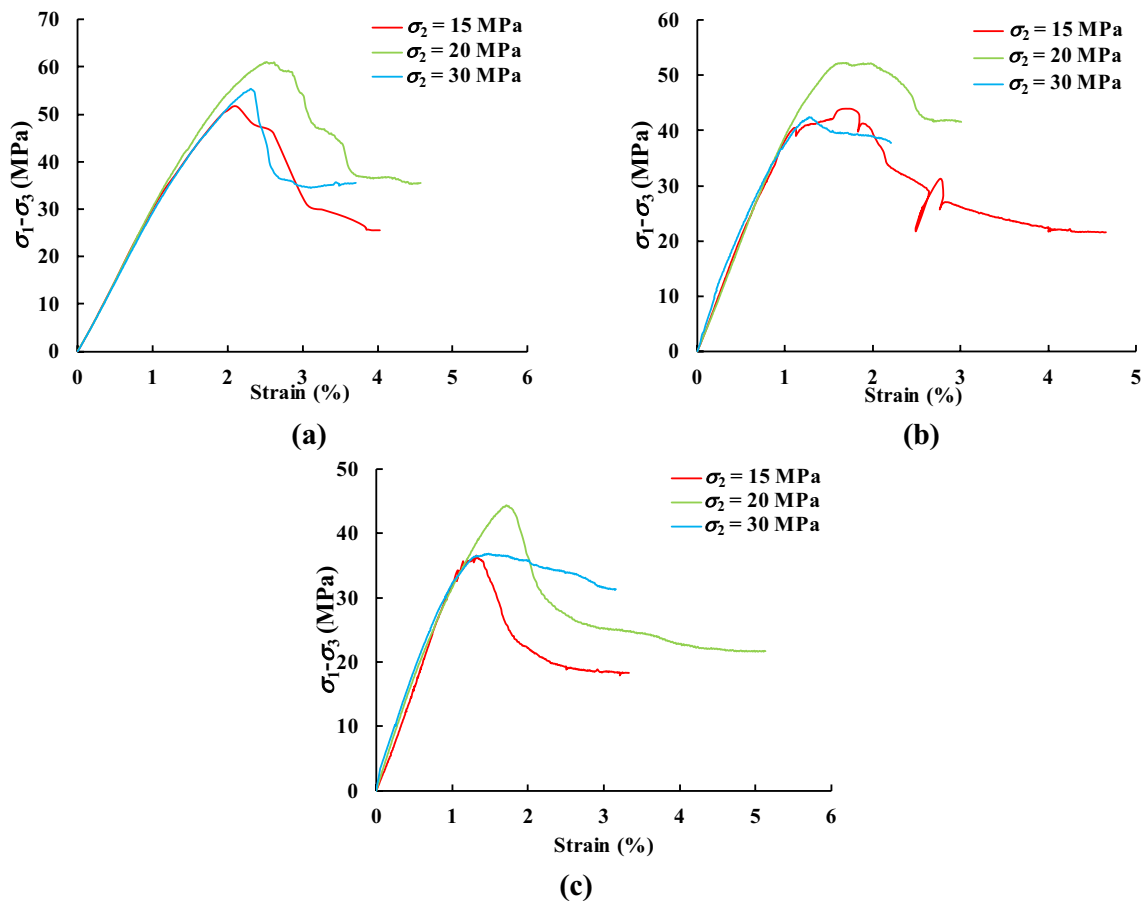
Fig. 4 Differential stress–strain curves of dry anisotropic coal samples under different true-triaxial loading conditions. **a** Bedding plane direction, **b** face cleat plane direction, and **c** butt cleat plane direction

transparent. From Figs. 6 and 7, two identifiable failure modes are observed for dry and water-saturated anisotropic coal samples subjected to true-triaxial stress compression: brittle shear and mixed splitting and shear failures. The failure modes of the dry coal samples were qualitatively similar to those of the water-saturated coal samples. In terms of observed shear failure, the final failure planes could be categorized as the single shear band, double shear bands, and conjugate shear bands. The traced failure plane always connected the top and bottom end face of the cubic coal sample. In addition, some local dilations and sliding failure due to preexisting cleats in the coal might also occurred in the failure plane. From the CT cross-sectional images across the $\sigma_1 - \sigma_3$ faces of the tested coal samples, the failure plane angles varied from test to test. As σ_2 increased from 15 to 30 MPa with a constant σ_3, the failure plane angle increased for each loading direction, and the failure plane gradually dipped in the σ_3 direction. A similar increase in the failure plane with σ_2 was found in sandstones tested under true-triaxial stress conditions (Haimson and Chang 2000; Ma and Haimson 2016). The failure modes of the coal samples were

different with the variations in loading directions relative to the weakness planes of the coal. When the coal samples were loaded in the butt cleat plane direction, shear failure was the dominant failure mode. When the coal samples were loaded in the face cleat plane or bedding plane directions, both shear failure and mixed splitting and shear failure were observed.

4 Discussion

4.1 The Effect of Water Weakening on the Mechanical Properties and Failure Behavior of Coal

The strength and stiffness characteristics of coal are of great fundamental importance in underground mining, since most potential coal seams are water saturated. The presence of water was found to significantly weaken the uniaxial compressive strength (UCS) and elastic modulus of sedimentary rocks, including coal (Hawkins and Mcconnell 1992; Vishal
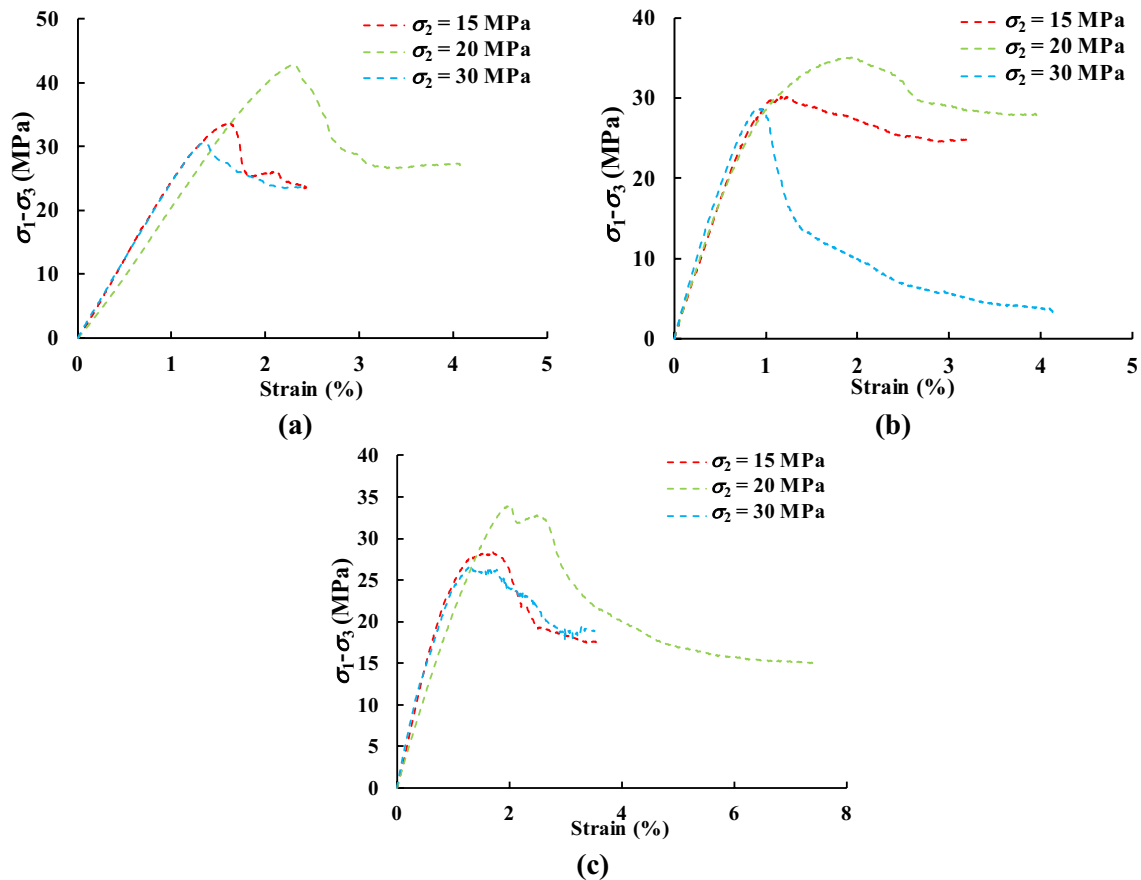
Fig. 5 Differential stress–strain curves of water-saturated anisotropic coal samples under different true-triaxial loading conditions. **a** Bedding plane direction, **b** face cleat plane direction, and **c** butt cleat plane direction

et al. 2015). The results tested under more realistic true-triaxial loading conditions were limited. Figure 8 shows the peak and elastic modulus of dry and water-saturated anisotropic coal samples under different true-triaxial loading conditions. The peak strength and elastic modulus of all the water-saturated coal samples were lower than those of the dry coal samples due to the water-weakening effect. Specifically, Fig. 9 presents the reduction in peak strength and elastic modulus of anisotropic coal samples after water adsorption under true-triaxial loading conditions. Due to the water adsorption, the peak strength of the coal was reduced by between 25.1 and 45.4% with a mean strength reduction of 33.4%, while the elastic modulus of the coal was reduced by between 5.9 and 34.5% with a mean elastic modulus reduction of 18.4% for different loading directions and true-triaxial loading conditions. The lower values of elastic modulus for water-saturated coal emphasize an increase in its ductile behavior. The coal strength and elastic modulus reduction under water saturation were higher than the results of low-rank coal, which were 16.8% and 7.6%, respectively (Perera et al. 2011). The difference in some physical attributes, such as preexisting cleat density between low-rank coal and

high-rank coal, could play an important role in the weaker weakening effect of coal (Vishal et al. 2015). The results obtained under true-triaxial stress conditions of this study were similar to the UCS reduction of water-saturated high-rank coal, with 27.2% obtained by Poulsen et al. (2014), indicating that the results were independent of stress conditions. The weakening effect of water on strength and elastic modulus may result from the reaction between water molecules and clay mineral content (i.e., kaolinite) within the coal matrix (Van Eeckhout 1976). After absorbing water, the water molecules can invade the clay minerals through preexisting cleats, and the associated swelling, softening, and disintegration phenomena occur (Erguler and Ulusay 2009). In addition, apart from the reaction with clay minerals, water also tends to form hydrogen bonds with the adsorbed water molecules and other surface chemical species (Busch and Gensterblum 2011), which leads to the structural rearrangement of coal and associated strength reduction. In addition, the presence of water could also reduce the specific surface energy and friction coefficient in coal, as reported in sandstones, magnifying the water-weakening effect (Baud et al. 2000). With regard to the failure behavior of the dry and

Table 3 Mean values of the peak and residual strength, axial strain at peak stress, elastic, and postpeak modulus of dry and water-saturated anisotropic coal samples under different true-triaxial stress conditions

Test number	Peak strength (MPa)	Residual strength (MPa)	Axial strain at peak stress (%)	Elastic modulus (GPa)	Postpeak modulus (GPa)
Coal-B-D15#	53.40	27.51	2.33	3.33	1.65
Coal-F-D15#	45.23	22.82	1.79	4.30	1.12
Coal-U-D15#	35.79	19.25	1.30	3.35	1.89
Coal-B-D20#	62.56	36.40	2.65	3.24	2.47
Coal-F-D20#	51.24	40.58	1.72	4.11	1.55
Coal-U-D20#	43.01	20.16	1.68	3.28	1.48
Coal-B-D30#	53.90	34.52	2.36	2.87	4.63
Coal-F-D30#	43.59	38.25	1.31	4.55	0.81
Coal-U-D30#	35.29	30.27	1.51	3.67	0.40
Coal-B-W15#	34.70	22.76	1.67	2.46	3.73
Coal-F-W15#	30.41	24.90	1.29	3.50	0.45
Coal-U-W15#	26.48	16.45	1.75	2.85	1.02
Coal-B-W20#	43.58	28.93	2.20	2.26	2.68
Coal-F-W20#	34.52	26.85	1.70	3.66	0.83
Coal-U-W20#	32.20	13.58	1.44	2.15	0.55
Coal-B-W30#	29.43	21.35	1.37	2.57	0.76
Coal-F-W30#	26.51	8.48	1.10	4.28	1.36
Coal-U-W30#	23.17	16.78	1.25	3.17	0.52

Test numbers refer to the dry and water-saturated coal samples tested under different conditions, i.e., Coal-B-D15# denotes the dry coal sample subjected to 15 MPa intermediate stress in the bedding plane direction

water-saturated coal samples, there were no significant differences in the failure modes before and after water adsorption of the coal.

4.2 The Effect of Intermediate Stress on the Mechanical Properties and Failure Behavior of Coal

According to the in situ stress measurements, true-triaxial stress conditions are more general and realistic (Zoback 1992; Kang et al. 2010). For specific underground reservoirs, such as coal seams, geological structures (i.e., faults and folds) are randomly distributed and might lead to high tectonic stress ($\sigma_2 > \sigma_3$) in the near regions. Understanding how the mechanical properties and failure behavior of coal evolve with intermediate stress is thus important for predicting the relevant field behavior of coal. In the commonly used conventional triaxial tests ($\sigma_2 = \sigma_3$), the strength of coal is enhanced with increasing confining pressure (Gao and Kang 2017), overlooking the effect of intermediate stress. Figure 10 shows the variations in σ_1 at failure with different σ_2 values of dry and water-saturated anisotropic coal samples. It can be seen that σ_1 at failure increased first with the increase in σ_2 and then decreased when the stress ratio σ_2/σ_1 exceeded 0.5, conflicting with results obtained under conventional triaxial loading conditions. A similar increasing then decreasing trend was also found in other sedimentary rocks (Fjær and Ruistuen 2002; Mogi 1967; Ma and

Haimson 2016). This trend was independent of the water adsorption or weakness plane orientations in the coal and could be well fitted by the polynomial equation of the second order. In underground coal mines, the postfailure behavior of coal is crucial to the support design. Figure 11 presents the variations in residual strength-to-peak strength ratios of coal under varying intermediate stresses. For both dry and water-saturated coal, the residual strength-to-peak strength ratios generally showed a linear increase with increasing intermediate stress, with only one exception of the strength data of water-saturated coal loaded in the face cleat plane direction. This means that the intermediate stress enhances the load bearing capability of the coal after failure. In Fig. 12, the field measurement results of coal pillars in underground coal mines also show a similar upward trend, where the ratios of the peak to residual strength of coal increased due to higher horizontal stress with distance into the pillar. According to the widely used Mohr–Coulomb failure criterion, the failure plane angle is constant and determined by the inherent properties of the rock materials. However, it is clear from Fig. 13 that the failure plane angle of both the dry and water-saturated samples increased with the intermediate stress, which could be fitted by a linear expression. Specifically, the failure plane angle of the dry coal samples loaded in the bedding plane direction increased by 19° with an intermediate stress increment of 15 MPa. In the face cleat and butt cleat directions, the failure plane angle of the dry coal samples increased by 8° and 16°, respectively, with intermediate

Fig. 6 CT scan cross-sectional and 3D reconstruction images of failure modes of dry anisotropic coal samples under different true-triaxial loading conditions: **a** bedding plane direction, **b** face cleat plane direction, and **c** butt cleat plane direction
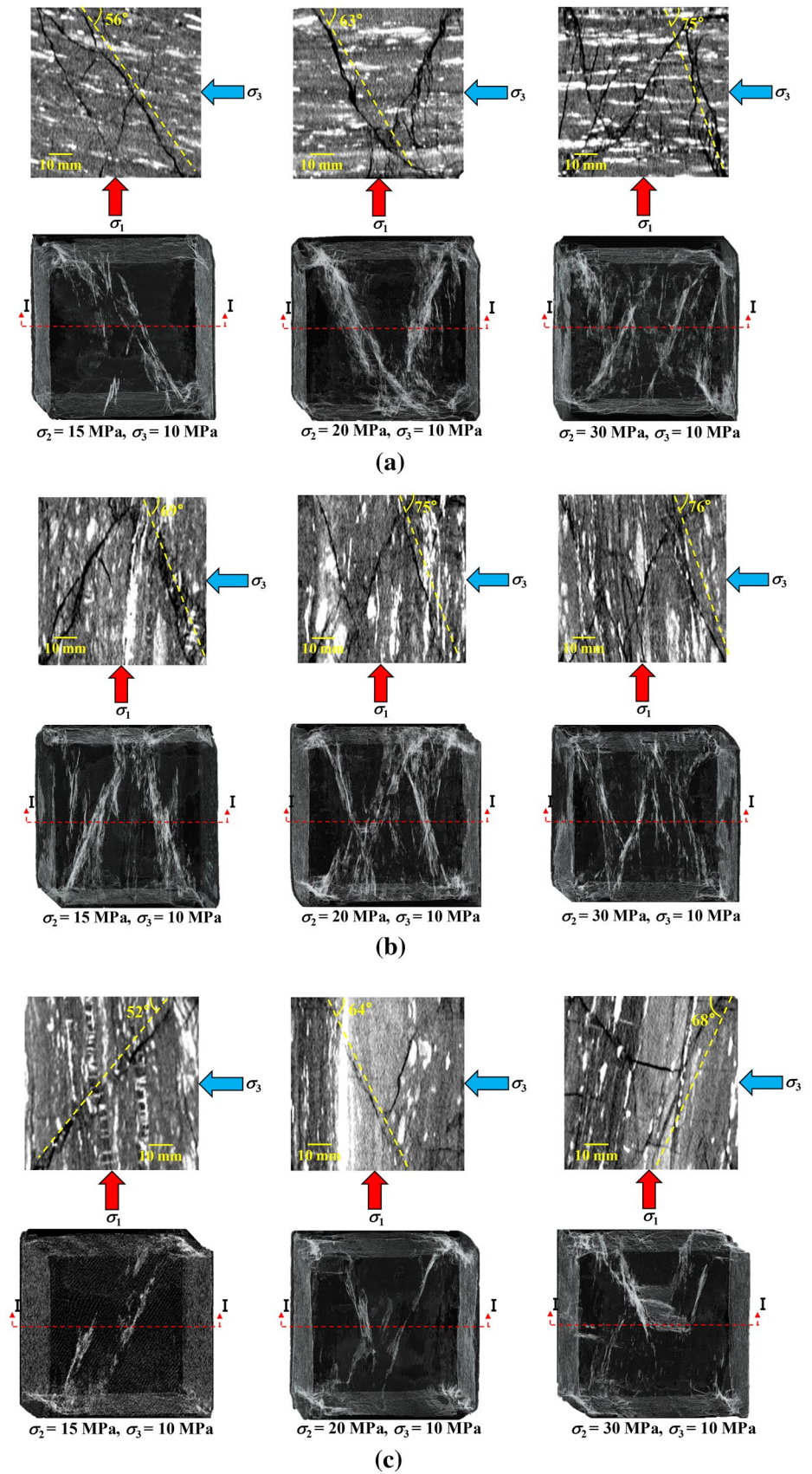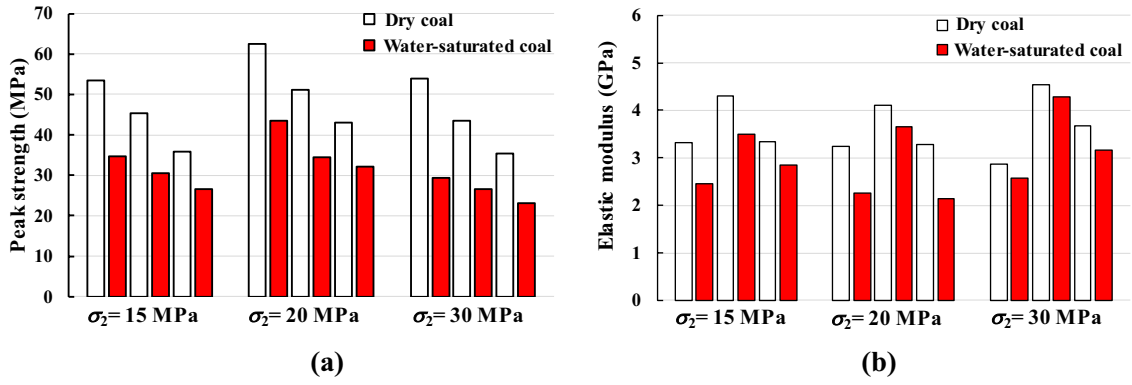
Fig. 7 CT scan cross-sectional and 3D reconstruction images of failure modes of water-saturated anisotropic coal samples under different true-triaxial loading conditions: **a** bedding plane direction, **b** face cleat plane direction, and **c** butt cleat plane direction
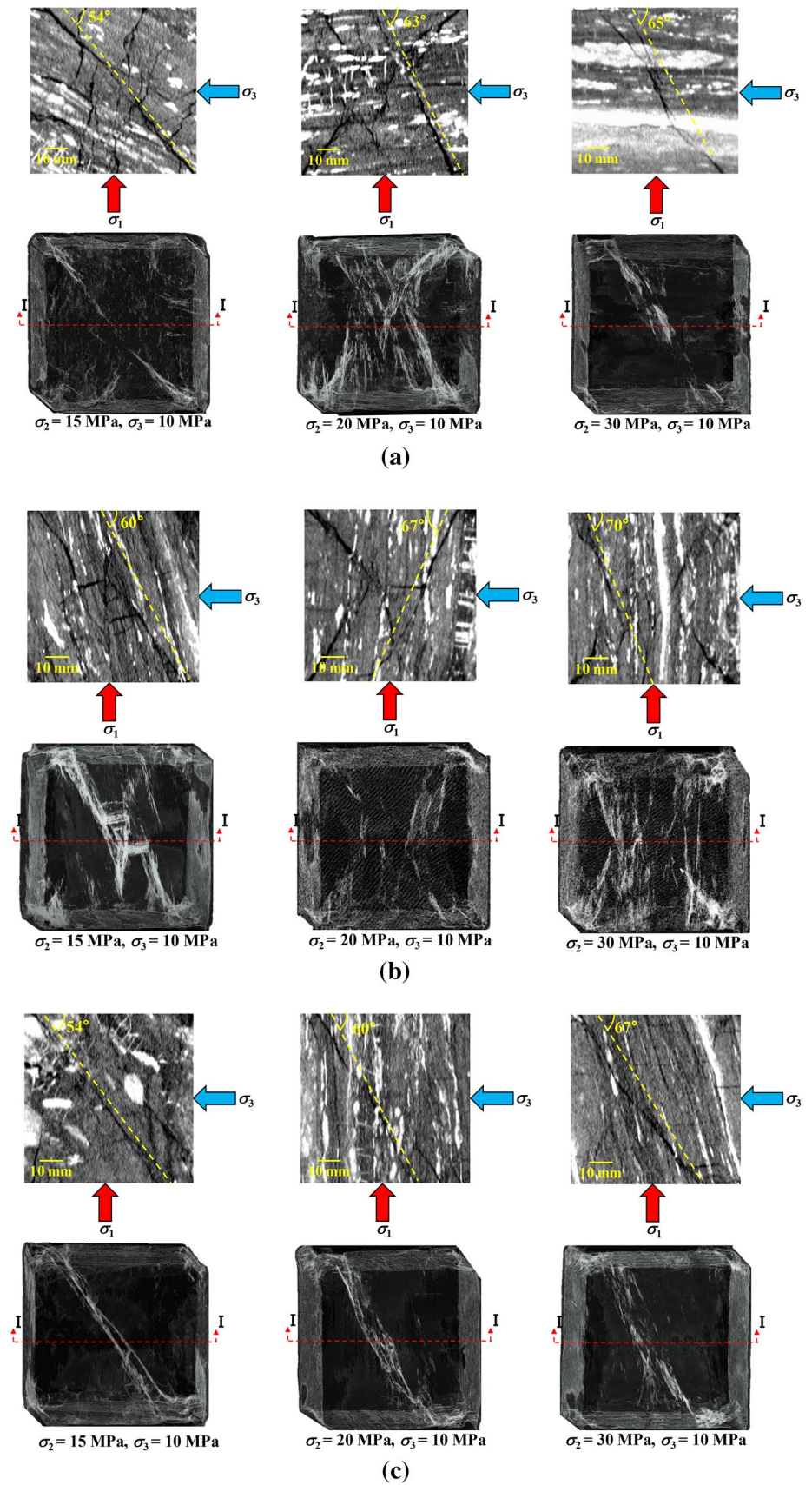
Fig. 8 Peak strength and elastic modulus of dry and water-saturated coal samples under different true-triaxial loading conditions. **a** Peak strength and **b** elastic modulus
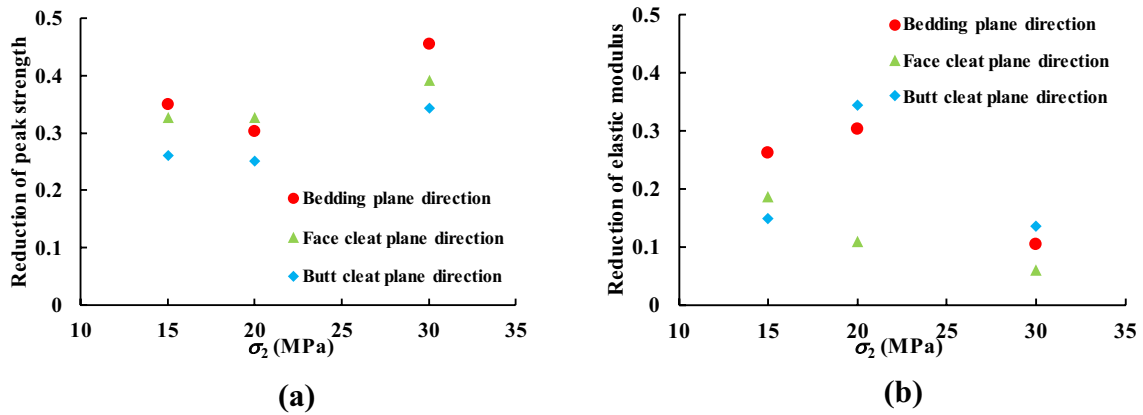
Fig. 9 Reduction in peak strength and elastic modulus of anisotropic coal samples after water adsorption under different true-triaxial loading conditions. **a** Reduction in peak strength and **b** reduction in elastic modulus
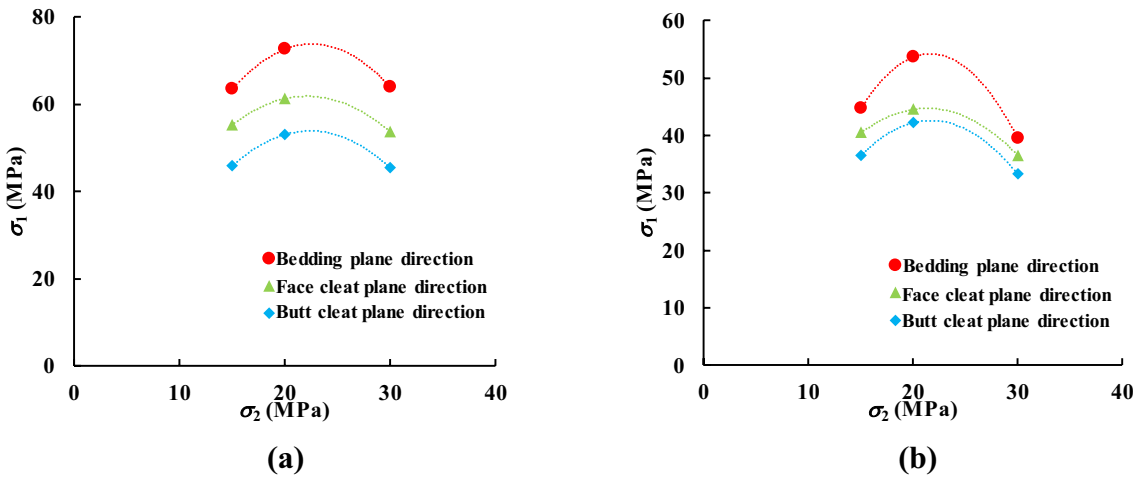
Fig. 10 Variations in σ_1 at failure with σ_2 of dry and water-saturated anisotropic coal samples. **a** Dry coal samples and **b** water-saturated samples
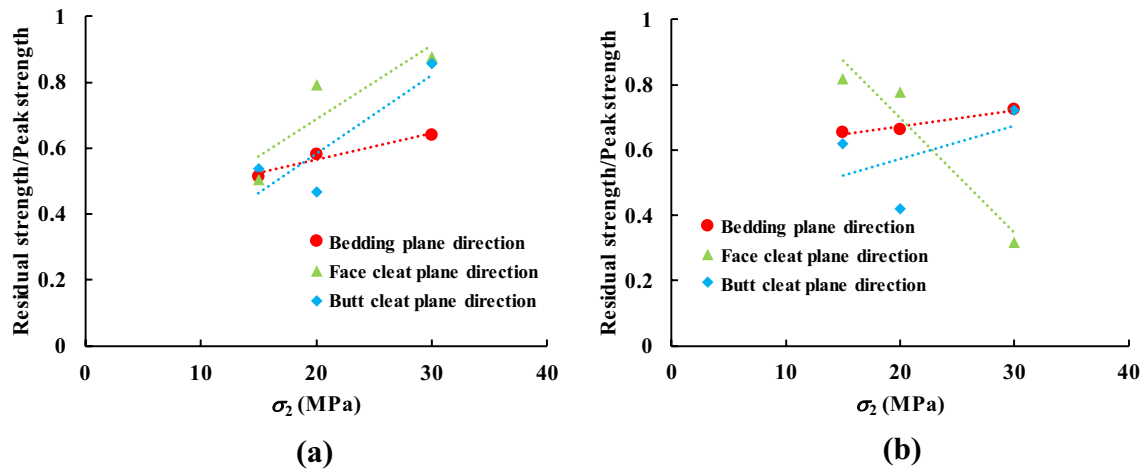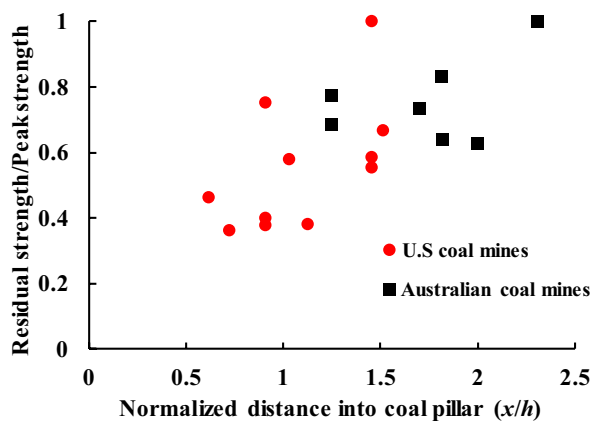
Fig. 11 Residual strength-to-peak strength ratios of dry and water-saturated anisotropic coal samples under varying intermediate stresses. **a** Dry coal samples and **b** water-saturated coal samples

stress increments of 15 MPa. Ma and Haimson (2016) also observed an increase in the failure angle with intermediate stress for dry sandstone subjected to true-triaxial stress. In comparison with their results, the increase in failure plane angles of dry coal is more significant with relatively low intermediate stress variations.

4.3 The Effect of Anisotropy on the Mechanical Properties and Failure Behavior of Coal

The tested coal samples contained preexisting anisotropic discontinuities, namely, the geometrically orthogonal bedding planes and face and butt cleats. Such weakness planes could affect the mechanical properties and failure behavior of the coal with orientation to the applied

Fig. 12 Variations in residual strength-to-peak strength ratio with normalized distance into the coal pillar, where x and h refer to the distance into the coal pillar and the coal pillar height, respectively (Li and Heasley 2014)

stress. To evaluate the effect of anisotropy, the ratios of strength and elastic modulus anisotropy of dry and water-saturated coal under different intermediate stresses are shown in Fig. 14. The vertical anisotropy is determined by the ratio of the strength and elastic modulus obtained in the bedding plane direction to the average values of the strength and elastic modulus obtained in both the face and butt cleat plane directions. The horizontal anisotropy is determined by the ratio of the strength and elastic modulus obtained in the face cleat direction to the strength and elastic modulus obtained in the butt cleat direction. For the coal strength, the vertical anisotropy is higher than the horizontal anisotropy under both dry and water-saturated conditions, regardless of variations in the intermediate stress. Meanwhile, both the vertical and horizontal strength anisotropy decreased after water adsorption. This meant that the water content within the coal samples might suppress the degree of anisotropy in terms of coal strength under true-triaxial loading conditions. For the elastic modulus of coal, the vertical anisotropy was lower than the horizontal anisotropy under both dry and water-saturated conditions, regardless of variations in intermediate stress. However, no significant decrease was observed in the elastic modulus anisotropy of the coal after water adsorption.

The brittleness is another key mechanical property of intact coal, because it is directly linked with the failure progress and coal mass response to mining activities in the field. Various expressions have been defined to quantify brittleness based on different concepts (Zhang et al. 2016; Feng et al. 2019). In this study, the coal brittleness is evaluated by the two brittleness indices based on the energy balance of the postpeak stage of the complete stress–strain curves (Tarasov and Potvin 2013). The brittleness index B_1 is determined
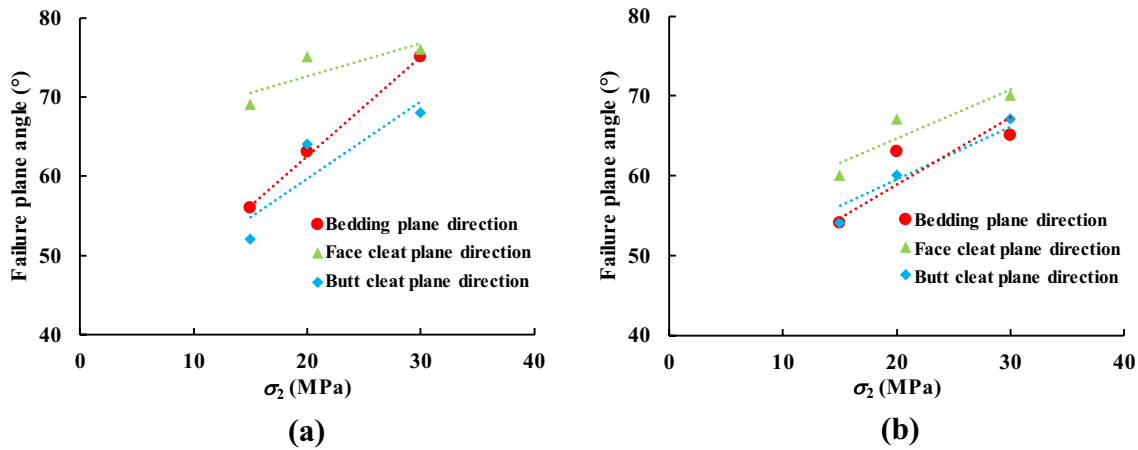
Fig. 13 Variations in the failure plane angle with intermediate stresses of dry and water-saturated coal samples. **a** Dry coal samples and **b** water-saturated coal samples
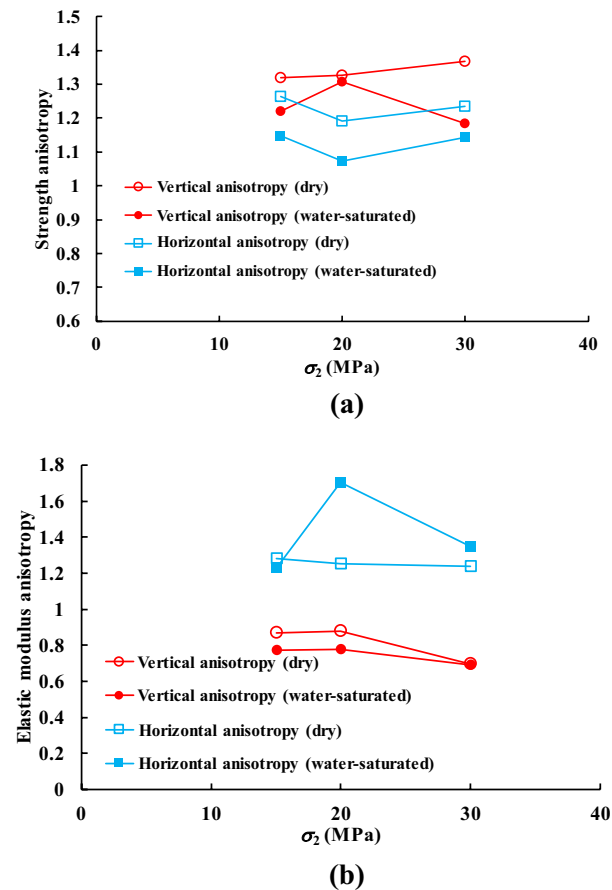

Fig. 14 Strength and elastic modulus anisotropy of dry and water-saturated coal under varying intermediate stresses. **a** Strength anisotropy and **b** elastic modulus anisotropy

by the ratio between the postpeak rupture energy and the withdrawn elastic energy and is described by the following equation:

$$B_1 = \frac{dW_r}{dW_e} = \frac{M - E}{M}, \tag{1}$$

where W_r is the postpeak rupture energy, W_e is the elastic energy, M is the postpeak modulus, and E is the elastic modulus.

The brittleness index B_2 represents the ratio between the released and the withdrawn elastic energy and is described by the following equation:

$$B_2 = \frac{dW_a}{dW_e} = \frac{E}{M}, \tag{2}$$

where W_a is the released energy.

As schematically shown in Fig. 15, the variations in brittleness indices B_1 and B_2 quantitatively describe the whole scale of brittleness from ductility to absolute brittleness, where the gray area and red area represent the postpeak rupture energy and the elastic energy, respectively. The failure behavior of rock could be classified as Class I and Class II according to the difference values of B_1 and B_2. The left part $(0 < B_1, B_2 < 1)$ belongs to the Class II self-sustained failure mode, while the right part $(1 < B_1 < +\infty$ or $-\infty < B_2 < 0)$ belongs to the Class I unspontaneous failure mode. Figure 16 shows the brittleness of dry and water-saturated anisotropic coal under varying intermediate stresses. All tested dry and water-saturated coal samples belong to the Class I unspontaneous failure mode $(1 < B_1 < +\infty$ or $-\infty < B_2 < 0)$. When the coal samples were loaded in the bedding plane direction, the brittleness of the coal was higher than when they were loaded in the other two cleat plane directions. This means that the coal samples could exhibit more violent failure when loaded in the bedding plane direction. High brittle minerals such as quartz distributed along the bedding planes of
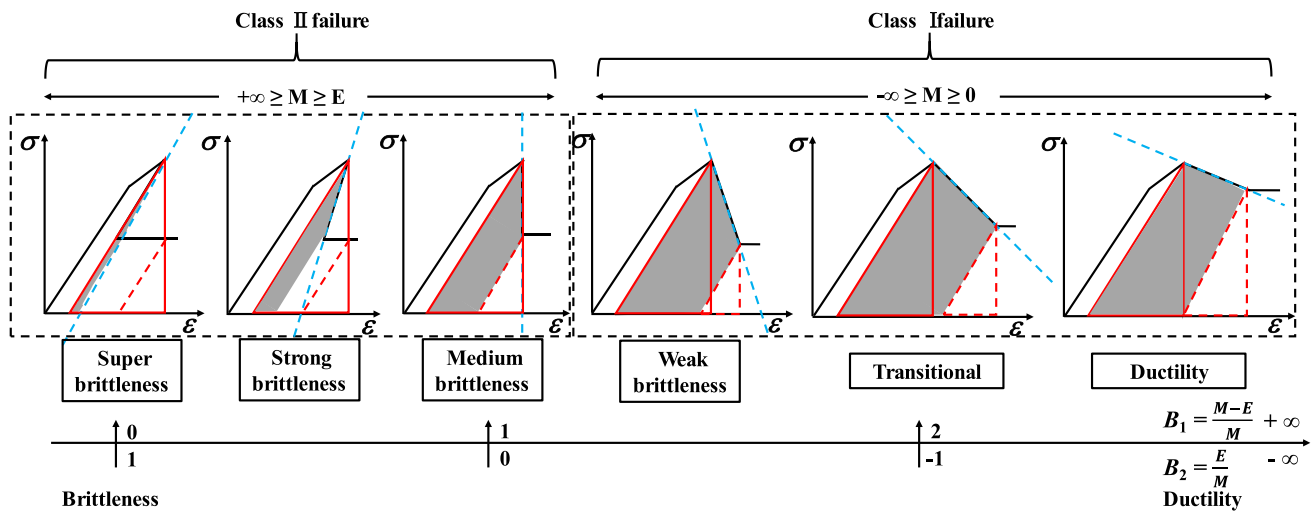
Fig. 15 Variations in the degree of brittleness characterized by the indices B_1 and B_2 with the complete stress–strain curves
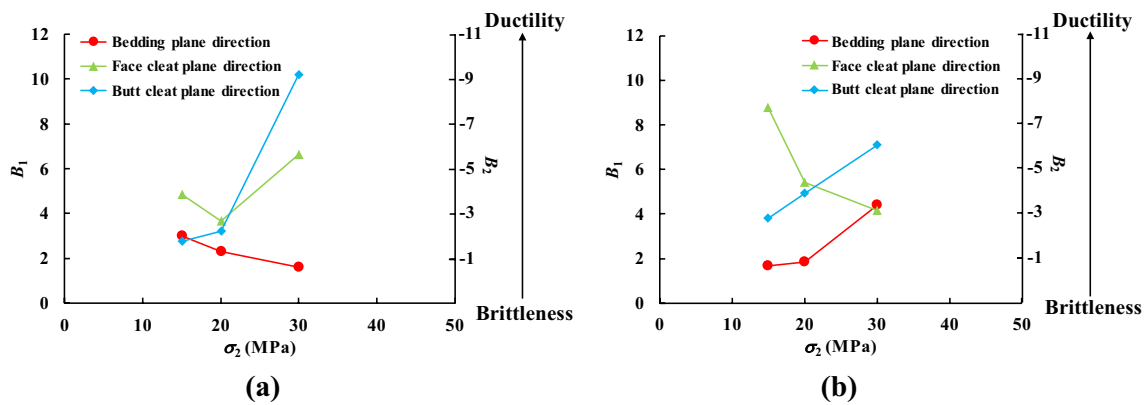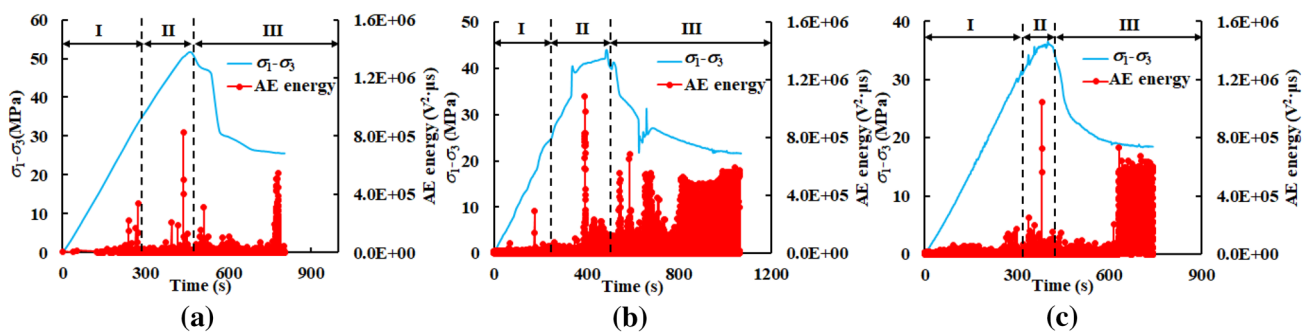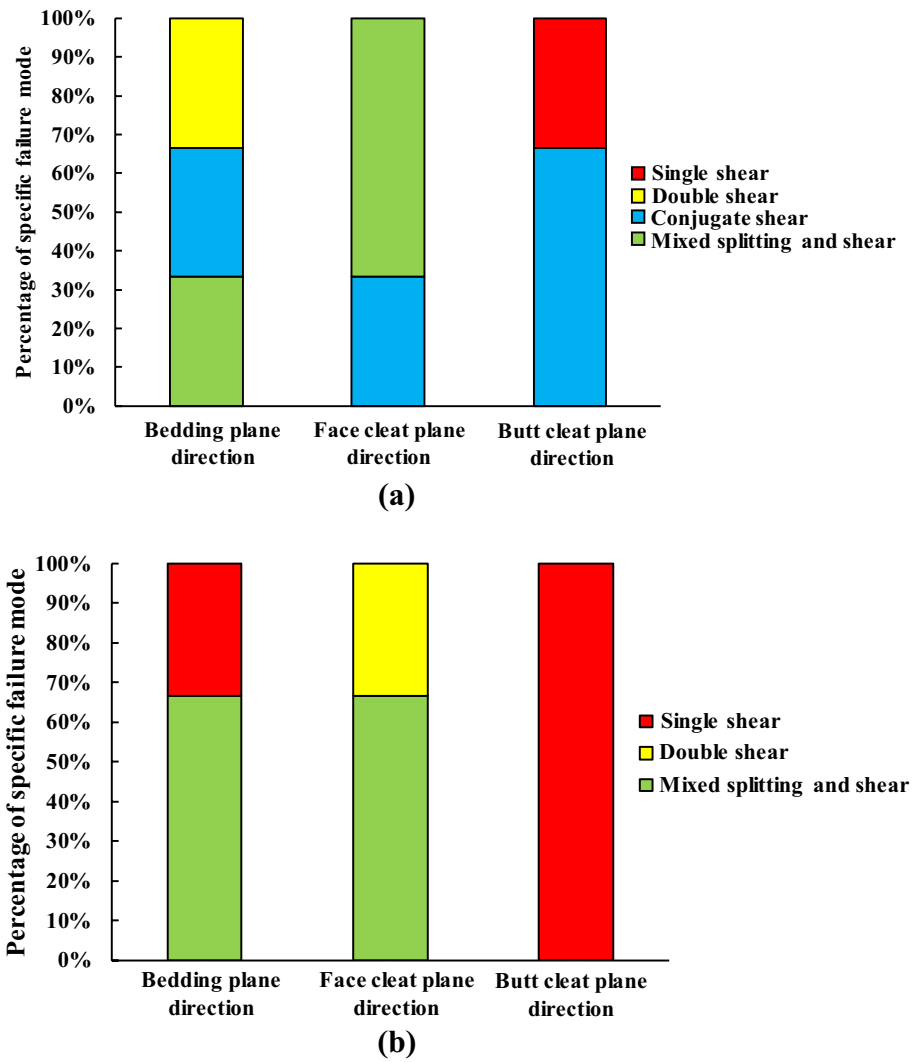

Fig. 16 Brittleness of dry and water-saturated anisotropic coal under varying intermediate stresses. **a** Dry coal samples and **b** water-saturated coal samples

the coal might be the reason for the higher brittleness of the coal when loaded in the bedding plane direction (Sibson 1977). When the coal samples were loaded in the butt cleat plane direction, the brittleness of the coal decreased with the intermediate stress. No significant change in the brittleness of the coal was observed before and after water adsorption. The percentage of the specific failure mode of the dry and water-saturated anisotropic coal samples is given in Fig. 17. The dominant failure mode of the anisotropic coal varied with the loading direction. When the coal samples were loaded in the bedding plane and face cleat directions, mixed splitting and shear failure were more generally observed, whereas most coal samples failed following the single shear failure mode when they were loaded in the butt cleat direction. In comparing the dry and water-saturated coal samples, the conjugate shear failure mode disappeared after water adsorption.

4.4 Evolution of AE Energy of Coal

Figures 18 and 19 show the AE energy–stress curves of the anisotropic dry and water-saturated coal samples under true-triaxial stress conditions. It can be seen that the evolution of AE energy of the anisotropic dry and water-saturated coal samples during the progressive failure can be divided into three following typical stages: the stable development of microcracks (stage I), the unstable development of macrofractures (stage II), and the postfailure region (stage III). In stage I, the differential stress increased quickly, while the AE energy increased slowly, which means that the microcracks steadily initiated and propagated. In stage II, the AE energy gradually increased and then experienced a significant rise when the coal samples were loaded to approach its peak strength, indicating that the microcracks were coalesced and propagated unstably until the macrofractures formed
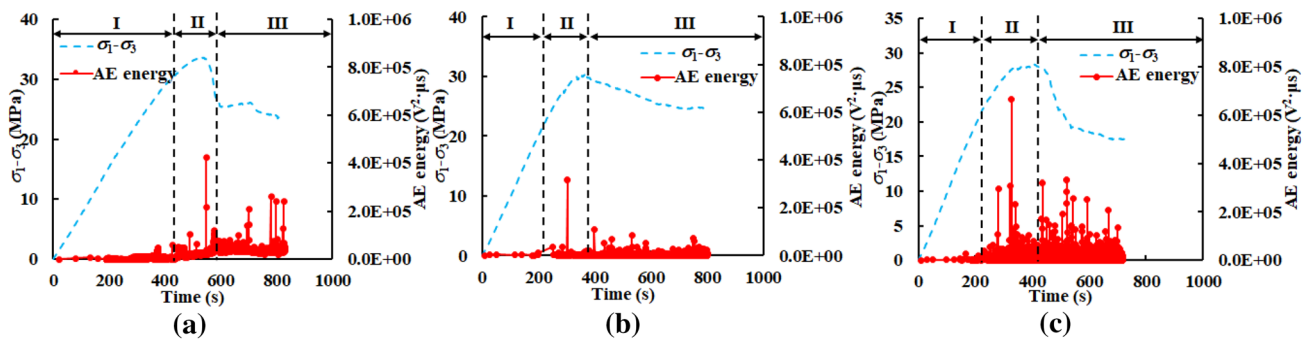
(a)

(b)

Fig. 18 AE energy–stress curves of anisotropic dry coal samples under true triaxial stress conditions of 15 MPa intermediate stress: **a** bedding plane direction, **b** face cleat plane direction, and **c** butt cleat plane direction

in the coal samples. In stage III, the AE energy gradu-
ally decreased and then increased when the coal samples
were loaded to the residual strength, suggesting that fric-
tional sliding between the newly developed macrofractures
controlled the postfailure region and led to the macroscopic
shear failure plane formation during this stage. For the
water-saturated coal samples, the AE energy was always
lower during the entire stages of coal progressive failure,

Fig. 19 AE energy–stress curves of anisotropic water-saturated coal samples under true triaxial stress conditions of 15 MPa intermediate stress: **a** bedding plane direction, **b** face cleat plane direction, and **c** butt cleat plane direction

and the AE characteristics were less pronounced in the postfailure region in comparison with dry coal samples. As discussed in Sect. 4.1, the presence of water could reduce the specific energy and friction coefficient of coal samples, leading to lower peak and residual strength of coal. Hence, less energy is required to induce the failure of coal, and the AE energy was less pronounced for the water-saturated coal samples during the stress loading process. Similar results of the water-weakening effect on AE characteristics were also found by Zhou et al. (2018) and Yao et al. (2016).

### 4.5 Identification of Failure Modes Using AE Characteristics of Coal

Figures 20, 21, and 22 show the cumulative AE counts ratio versus time curves of the dry and water-saturated coal samples loaded in different directions. A strong correlation between failure modes and AE characteristic curves can be observed. For the coal samples that failed in the shearing modes, there were few AE events at the beginning of the loading, and most AE events occurred at or very close to the

final failure. For the coal samples that failed in the mixed splitting and shearing modes, the coal samples had more AE events at the beginning of the loading and throughout the whole loading process, which showed steady linear growth of the AE events. This difference in the patterns of the AE curves could be used to distinguish the two failure modes of the coal that appeared in these true-triaxial compression tests. Specifically, when the coal samples were loaded in the bedding plane and face cleat plane directions, two types of AE patterns were observed, since both shearing and mixed splitting and shear modes occurred. In the case of the shearing failure, which was observed for the coal samples loaded in the butt cleat plane direction, only the shear failure AE pattern occurred.

To reveal the fracture mechanism of dry and water-saturated coal samples under true-triaxial stress conditions, the microcrack patterns were further identified based on the AE parameters. The average frequency (AF) value and rise time/amplitude (RA) value are directly associated with the microcrack patterns (Aggelis 2011) and are used to classify the microcrack patterns in this study. In
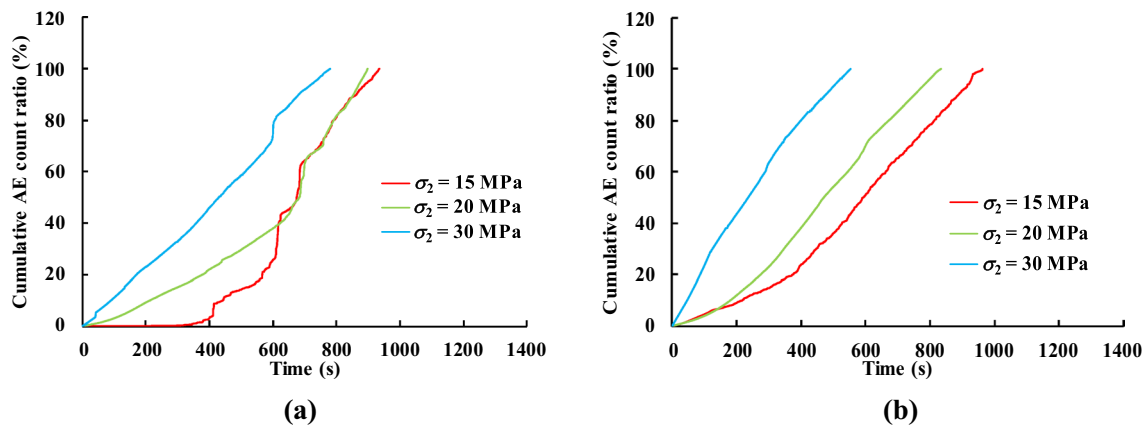
Fig. 20 Cumulative AE count ratio versus time curves of dry and water-saturated coal samples loaded in the bedding plane direction. **a** Dry coal samples and **b** water-saturated coal samples
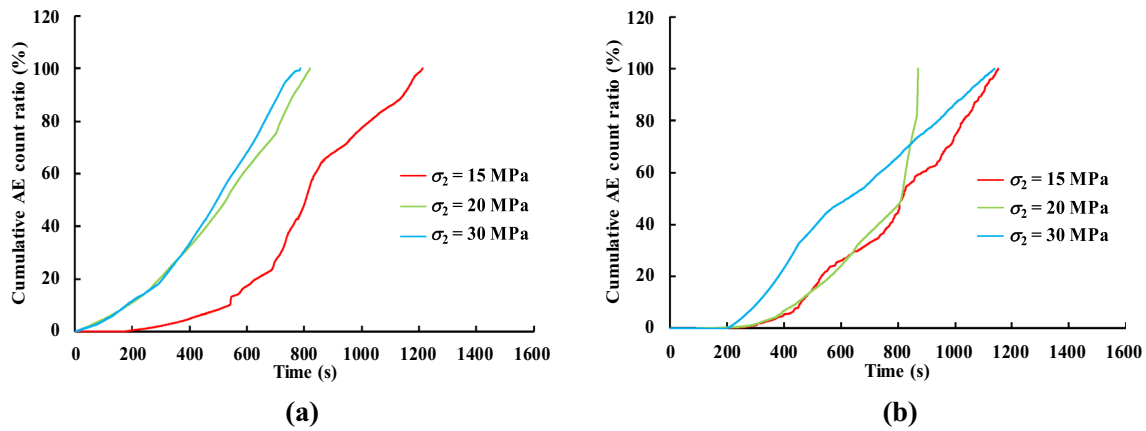
Fig. 21 Cumulative AE count ratio versus time curves of dry and water-saturated coal samples loaded in the face cleat plane direction. **a** Dry coal samples and **b** water-saturated coal samples
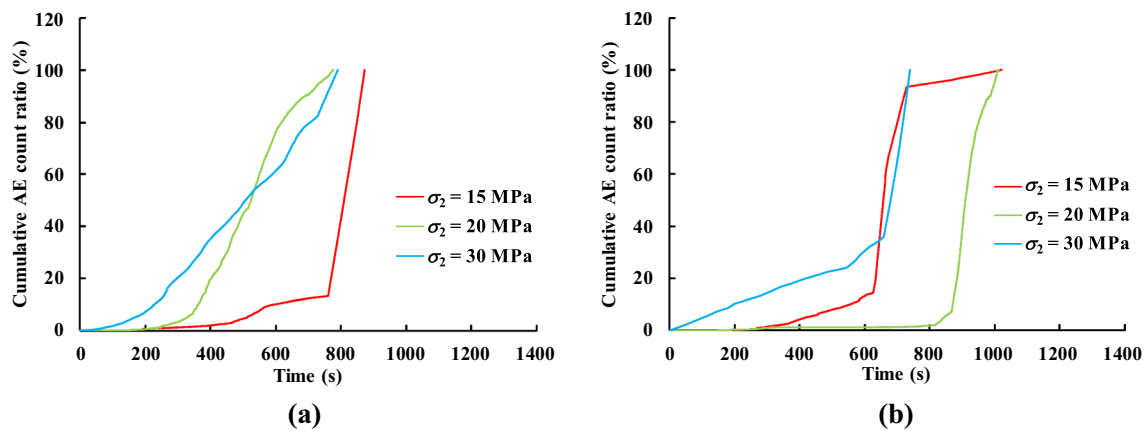

Fig. 22 Cumulative AE count ratio versus time curves of dry and water-saturated coal samples loaded in the butt cleat plane direction. **a** Dry coal samples and **b** water-saturated coal samples

particular, the AF value is calculated by the ratio of AE counts to the duration time of the AE signal, and the RA value is calculated as the rise time (delay between the onset and maximum amplitude) divided by the amplitude. The proportion of the AF to RA values generally has a diploid relationship (Grosse and Ohtsu 2008; Yao et al. 2019; Lu et al. 2018). An AE signal with a low AF value and a high RA value normally corresponds to the shearing cracks, whereas a signal with a high AF value and a low RA value represents the tensile cracks (Ohno and Ohtsu 2010). Figures 23 and 24 show the correlation plots between the AF and RA values of the anisotropic dry and water-saturated coal samples under true-triaxial stress conditions of 15 MPa intermediate stress. For the coal samples loaded in the bedding plane and face cleat plane directions, the percentages of tensile cracks were slightly higher than the percentages of shear cracks, which means that both tensile and shear cracks were initiated and propagated but tensile cracking was preferential during the failure progress. For the coal samples loaded in the butt cleat plane direction, more shear cracks and many fewer tensile cracks were identified than in the coal samples loaded in the other two directions, which indicates that coal samples mainly experienced shear crack growth during the failure progress. Hence, as verified by the CT cross-sectional and 3D reconstruction images in Figs. 6 and 7, both the splitting and shear failure planes were formed macroscopically in the coal samples loaded in the bedding plane and face cleat plane directions, whereas coal samples loaded in the butt cleat plane exhibited shear failure macroscopically. In addition, in comparison with dry coal samples, the ratios of shear cracks during progressive failure is higher for water-saturated coal samples, induced by the reduction in friction coefficient and less constrained movement along cracks due to the presence of water (Eberhardt et al. 1999; Zhang and Gao 2015).
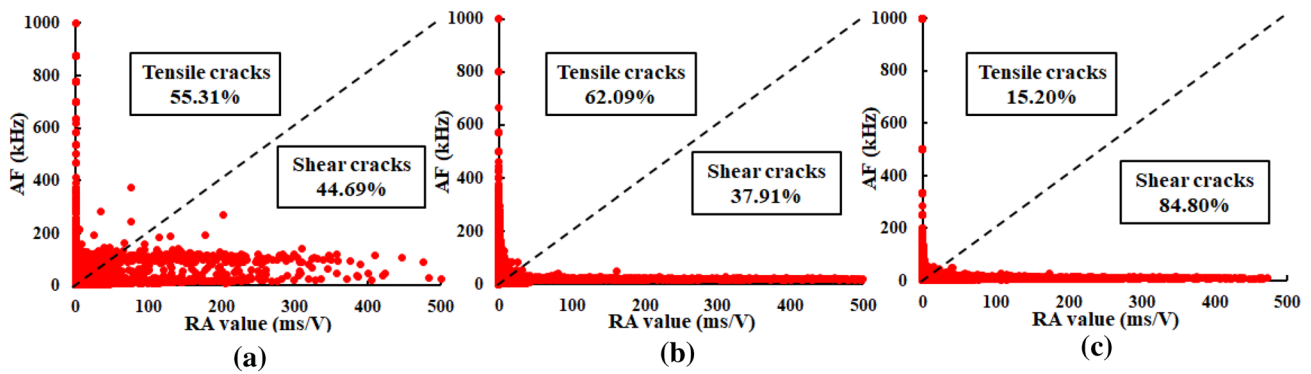
Fig. 23 Plots of the correlation between the AF and RA values in the progressive failure process of anisotropic dry coal samples under true tri-axial stress conditions of 15 MPa intermediate stress: **a** bedding plane direction, **b** face cleat plane direction, and **c** butt cleat plane direction
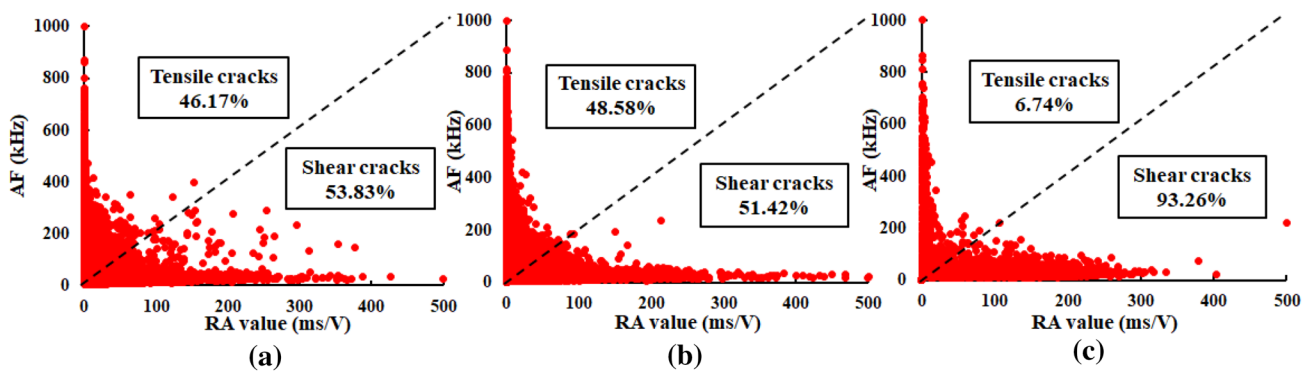
Fig. 24 Plots of the correlation between the AF and RA values in the progressive failure process of anisotropic water-saturated coal samples under true triaxial stress conditions of 15 MPa intermediate stress: **a** bedding plane direction, **b** face cleat plane direction, and **c** butt cleat plane direction

4.6 Implications for Underground Coal Mine Field Applications

Underground coal mines are generally undertaken in high geo-stress areas, where failure of the coal is generally una-voidable due to high stress concentrations within the coal body during frequent mining. By monitoring the AE sig-nal variations, failure modes of the coal could be recog-nized and predicted, which is beneficial to burst control. Most underground coal seams are generally saturated with large amounts of water, especially in the regions treated by hydraulic stimulation (Lu and Wang 2015; Zhang and Shen 2004). The presence of water could significantly reduce the strength and deformability of the coal. When coal mining is near high tectonic regions, the coal peak strength might be lower, but the ratio of the residual strength-to-peak strength is increased due to relatively high intermediate stresses. The anisotropic preexisting natural weakness planes could also have a great influence on the variations in the mechani-cal properties and failure behavior of the coal. Thus, when

determining the coal support parameters and burst control methods, special attention should be paid to both the outer environmental factors (i.e., structure folds and water intru-sion) and the internal anisotropic structure of the coal. The laboratory scale used in the current study is limited to the centimeter level, and a larger scale of coal samples should be implemented in future studies to improve applications in the field.

5 Conclusions

In this study, experimental data on the mechanical prop-erties and failure behavior of both dry and water-saturated anisotropic coal samples under different true-triaxial loading conditions were presented. The effects of water weakening, intermediate stress and structural anisotropy on the mechani-cal properties and failure behavior of coal were systemati-cally analyzed and discussed. The following main findings could be drawn:

The presence of water in the tested high-rank coal samples has a great influence on the mechanical properties of the coal. The peak strength of the coal was reduced by between 25.1 and 45.4% with a mean strength reduction of 33.4%, while the elastic modulus of the coal was reduced by between 5.9 and 34.5% with a mean elastic modulus reduction of 18.4% for different loading directions and true-triaxial loading conditions. After water adsorption, both the vertical and horizontal strength anisotropy decreased, while no significant decrease was found in the elastic modulus anisotropy. The failure modes of the dry coal samples were qualitatively similar to those of the water-saturated coal samples.

Intermediate stress plays an important role in determining both the mechanical properties and the failure behavior of coal. The maximum stress at failure first increased with increasing intermediate stress and then decreased when the stress ratio of the intermediate stress to maximum stress exceeded 0.5, conflicting with the results obtained under conventional triaxial loading conditions. This trend is independent of the water adsorption and cleat orientations of the coal. The residual strength-to-peak strength ratios and the failure plane angles showed a linear increase with increasing intermediate stress.

All the tested dry and water-saturated coal samples belong to the Class I unspontaneous failure mode with relatively low brittleness. When the coal samples were loaded in the bedding plane direction, the brittleness of the coal was higher than when they were loaded in the other two cleat plane directions. When the coal samples were loaded in the butt cleat plane direction, the brittleness of the coal decreased with the intermediate stress.

Two typical failure modes of the dry and water-saturated coal were observed: shear and mixed splitting and shear failures. The dominant failure mode of the coal varied with the loading direction relative to the weakness planes. When the coal samples were loaded in the bedding plane and face cleat directions, mixed splitting and shear failures were more generally observed, whereas most coal samples failed following the single shear failure mode when they were loaded in the butt cleat direction. Microshear cracks were dominantly detected when the coal samples were loaded in the butt cleat plane direction. The two typical failure modes of the coal could be well recognized and predicted by the AE characteristic curves.

Compliance with Ethical Standards

References

Aggelis DG (2011) Classification of cracking mode in concrete by acoustic emission parameters. Mech Res Commun 38(3):153–157

Baud P, Zhu W, Wong TF (2000) Failure mode and weakening effect of water on sandstone. J Geophys Res 105:16371–16389

Browning J, Meredith P, Stuart C, Healy D, Harland S, Mitchell T (2017) Acoustic characterization of crack damage evolution in sandstone deformed under conventional and true-triaxial loading. J Geophys Res Solid Earth 122(6):4395–4412

Busch A, Gensterblum Y (2011) CBM and CO_2-ECBM related sorption processes in coal: a review. Int J Coal Geol 87:49–71

Duan M, Jiang C, Gan Q, Li M, Peng K, Zhang W (2019) Experimental investigation on the permeability, acoustic emission and energy dissipation of coal under tiered cyclic unloading. J Nat Gas Sci Eng. https://doi.org/10.1016/j.jngse.2019.103054

Eberhardt E, Stimpson B, Stead D (1999) Effects of grain size on the initiation and propagation thresholds of stress-induced brittle fractures. Rock Mech Rock Eng 32(2):81–99

Erguler ZA, Ulusay R (2009) Water-induced variations in mechanical properties of clay-bearing rocks. Int J Rock Mech Min Sci 46:355–370

Feng R, Zhang Y, Rezagholilou A, Roshan H, Sarmadivaleh M (2019) Brittleness Index: from conventional to hydraulic fracturing energy model. Rock Mech Rock Eng. https://doi.org/10.1007/s00603-019-01942-1

Fjær E, Ruistuen H (2002) Impact of the intermediate principal stress on the strength of heterogeneous rock. J Geophys Res Solar Earth. https://doi.org/10.1029/2001JB000277

Gao F, Kang H (2017) Experimental study on the residual strength of coal under low confinement. Rock Mech Rock Eng 50:285–296

Grosse CU, Ohtsu M (2008) Acoustic emission testing. Springer, Berlin

Haimson B, Chang C (2000) A new true-triaxial cell for testing mechanical properties of rock, and its use to determine rock strength and deformability of Westerly granite. Int J Rock Mech Min Sci 37(1–2):285–296

Hawkins AB, Mcconnell BJ (1992) Sensitivity of sandstone strength and deformability to changes in moisture-content. Q J Eng Geol 25:115–130

Jia J, Wang H, Tang J, Li X, Li K, Hu G (2006) Determination of key strata and interval of roofing breaking of hard and soft composite roofs. Chin J Rock Mech Eng 25(5):974–978 **(in Chinese)**

Jiang C, Niu B, Yin G, Zhang D, Yu T, Wang P (2019) CT-based 3D reconstruction of the geometry and propagation of hydraulic fracturing in shale. J Petrol Sci Eng 179:899–911

Kang H, Zhang X, Si L, Wu Y, Gao F (2010) In situ stress measurements and stress distribution characteristics in underground coal mines in China. Eng Geol 116:333–345

Kong X, Wang E, Hu S, Shen R, Li X, Zhan T (2016) Fractal characteristics and acoustic emission of coal containing methane in triaxial compression failure. J Appl Geophys 124:139–147

Kong R, Feng X-T, Zhang X, Yang C (2018) Study on crack initiation and damage stress in sandstone under true-triaxial compression. Int J Rock Mech Min Sci 106:117–123

Kwaśniewski M, Rodríguez-Oitaben P (2009) Effect of water on the deformability of rocks under uniaxial compression. ISRM regional symposium EUROCK 2009 rock engineering in different ground conditions-soft rock and karst. Dubrovnik, Cavtat, pp 271–276

Laubach S, Marrett R, Olson J, Scott A (1998) Characteristics and origins of coal cleat: a review. J Coal Geol 35(1–4):175–207

Li K, Heasley K (2014) Using field measurements to quantify the post-failure behavior of coal. In: Proceedings of the 49th US rock mechanics/geomechanics symposium, San Francisco, p 7

Li D, Wong LNY, Liu G, Zhang X (2012) Influence of water content and anisotropy on the strength and deformability of low porosity meta-sedimentary rocks under triaxial compression. Eng Geol 126(1):46–66

Li Y, Zhang J, Liu Y (2016) Effects of loading direction on failure load test results for Brazilian tests on coal rock. Rock Mech Rock Eng 49(6):2173–2180

Li D, Wang E, Kong X, Wang X, Zhang C, Jia H, Wang H, Qian J (2018) Fractal characteristics of acoustic emissions from coal under multi-stage true-triaxial compression. J Geophys Eng 15(5):2021–2032

Li D, Wang E, Kong X, Ali M, Wang D (2019) Mechanical behaviors and acoustic emission fractal characteristics of coal specimens with a pre-existing flaw of various inclinations under uniaxial compression. Int J Rock Mech Min Sci 116:38–51

Liu X, Tan Y, Ning J, Lu Y, Gu Q (2018a) Mechanical properties and damage constitutive model of coal in coal-rock combined body. Int J Rock Mech Min Sci 110:140–150

Liu Y, Li M, Yin G, Zhang D, Deng B (2018b) Permeability evolution of anthracite coal considering true-triaxial stress conditions and structural anisotropy. J Nat Gas Sci Eng 52:492–506

Liu S, Li X, Li Z, Chen P, Yang X, Liu Y (2019a) Energy distribution and fractal characterization of acoustic emission (AE) during coal deformation and fracturing. Measurement 136:122–131

Liu S, Li X, Wang D, Wu M, Yin G, Li M (2019b) Mechanical and acoustic emission characteristics of coal at temperature impact. Nat Res Res. https://doi.org/10.1007/s11053-019-09562-w

Liu Y, Yin G, Li M, Zhang D, Deng B, Liu C, Lu J (2019c) Anisotropic mechanical properties and the permeability evolution of cubic coal under true-triaxial stress paths. Rock Mech Rock Eng 2019:1–17

Liu Y, Yin G, Zhang D, Li M, Deng B, Liu C, Yin S (2019d) Directional permeability evolution in intact and fractured coal subjected to true-triaxial stresses under dry and water-saturated conditions. Int J Rock Mech Min Sci 119:22–34

Lu Y, Wang L (2015) Numerical simulation of mining-induced fracture evolution and water flow in coal seam floor above a confined aquifer. Comput Geotech 67:157–171

Lu Y, Li W, Wang L, Li Z, Meng X, Wang B, Zhang K (2018) Damage evolution and failure behavior of sandstone under true-triaxial compression. Geotech Test J 42(3):610–637

Ma X, Haimson B (2016) Failure characteristics of two porous sandstones subjected to true-triaxial stresses. J Geophys Res Solid Earth 121(9):6477–6498

Mark C, Gauna M (2016) Evaluating the risk of coal bursts in underground coal mines. Int J Min Sci Technol 26:47–52

Minaeian V, Dewhurst DN, Rasouli V (2017) Deformational behaviour of a clay-rich shale with variable water saturation under true-triaxial stress conditions. Geomech Energy Environ 11:1–13

Mogi K (1967) Effect of the intermediate principal stress on rock failure. J Geophys Res 72:5117–5131

Ohno K, Ohtsu M (2010) Crack classification in concrete based on acoustic emission. Constr Build Mater 24:2339–2346

Paul S, Chatterjee R (2011) Determination of in situ stress direction from cleat orientation mapping for coal bed methane exploration in south-eastern part of Jharia coalfield, India. Int J Coal Geol 87:87–96

Perera M, Ranjith P, Peter M (2011) Effects of saturation medium and pressure on strength parameters of Latrobe Valley brown coal: carbon dioxide, water and nitrogen saturations. Energy 36(12):6941–6947

Poulsen B, Shen B, Williams D, Huddlestone-Holmes C, Erarslan N, Qin J (2014) Strength reduction on saturation of coal and coal measures rocks with implications for coal pillar strength. Int J Rock Mech Min Sci 71:41–52

Prikryl R, Lokajicek T, Li C, Rudajev V (2003) Acoustic emission characteristics and failure of uniaxially stressed granitic rocks: the effect of rock fabric. Rock Mech Rock Eng 36:255–270

Ranjith PG, Perera MSA (2012) Effects of cleat performance on strength reduction of coal in CO_2 sequestration. Energy 45(1):1069–1075

Scholtès L, Donze F-V, Khanal M (2011) Scale effects on strength of geomaterials, case study: coal. J Mech Phys Solids 59:1131–1146

Sibson RH (1977) Fault rocks and fault mechanisms. J Geol Soc 133:191–213

Tarasov B, Potvin Y (2013) Universal criteria for rock brittleness estimation under triaxial compression. Int J Rock Mech Min Sci 59:57–69

Van Eeckhout EM (1976) The mechanisms of strength reduction due to moisture in coal mine shale. Int J Rock Mech Min Sci Geomech Abstr 13:61–67

Vásárhelyi B, Van P (2006) Influence of water content on the strength of rock. Eng Geol 84:70–74

Vishal V, Ranjith PG, Singh TN (2015) An experimental investigation on behaviour of coal under fluid saturation, using acoustic emission. J Nat Gas Sci Eng 22:428–436

Wang S, Elsworth D, Liu J (2013) Permeability evolution during progressive deformation of intact coal and implications for instability in underground coal seams. Int J Rock Mech Min Sci 58:34–45

Wasantha PLP, Ranjith PG (2014) Water-weakening behavior of Hawkesbury sandstone in brittle regime. Eng Geol 178:91–101

Wong LNY, Maruvanchery V, Liu G (2015) Water effects on rock strength and stiffness degradation. Acta Geotech 11(4):713–737

Xu T, Zhou G, Heap MJ, Yang S, Konietzky H, Baud P (2018) The modeling of time-dependent deformation and fracturing of brittle rocks under varying confining and pore pressures. Rock Mech Rock Eng 51(10):3241–3263

Yang S, Jing H, Wang S (2012) Experimental investigation on the strength, deformability, failure behavior and acoustic emission locations of red sandstone under triaxial compression. Rock Mech Rock Eng 45(4):583–606

Yao Q, Chen T, Ju M, Liang S, Liu Y, Li X (2016) Effects of water intrusion on mechanical properties of and crack propagation in coal. Rock Mech Rock Eng 49:4699–4709

Yao Q, Chen T, Tang C, Sedighi M, Wang S, Huang Q (2019) Influence of moisture on crack propagation in coal and its failure modes. Eng Geol 258:105–156

Yin G, Li M, Wang J, Li W (2015) Mechanical behavior and permeability evolution of gas infiltrated coals during protective layer mining. Int J Rock Mech Min Sci 80:292–301

Zhang Z, Gao F (2015) Experimental investigation on the energy evolution of dry and water-saturated red sandstones. Int J Min Sci Technol 25(3):383–388

Zhang J, Shen B (2004) Coal mining under aquifers in China: a case study. Int J Rock Mech Min Sci 41:629–639

Zhang D, Ranjith PG, Perera MSA (2016) The brittleness indices used in rock mechanics and their application in shale hydraulic fracturing: a review. J Pet Sci Eng 143:158–170

Zhang D, Yang Y, Chu Y, Zhang X, Xue Y (2018a) Influence of loading and unloading velocity of confining pressure on strength and permeability characteristics of crystalline sandstone. Results Phys 9:1363–1370

Zhang J, Ai C, Li Y, Che M, Gao R, Zeng J (2018b) Energy-based brittleness index and acoustic emission characteristics of anisotropic coal under triaxial stress condition. Rock Mech Rock Eng 51:3343–3360

Zhao Y, Liu S, Jiang Y, Wang K, Huang Y (2016) Dynamic tensile strength of coal under dry and saturated conditions. Rock Mech Rock Eng 49(5):1709–1720

Zhao T, Guo W, Tan Y, Yin Y, Cai L, Pan J (2018) Case studies of rock bursts under complicated geological conditions during multi-seam mining at a depth of 800 m. Rock Mech Rock Eng 51:1539–1564

Zhou Z, Cai X, Ma D, Cao W, Chen L, Zhou J (2018) Effects of water content on fracture and mechanical behavior of sandstone with a low clay mineral content. Eng Fract Mech 193:47–65

Zoback ML (1992) First-and second-order patterns of stress in the lithosphere: the World Stress Map Project. J Geophys Res 97(B8):11703–11728

Publisher's Note Springer Nature remains neutral with regard to jurisdictional claims in published maps and institutional affiliations.